Measuring Substrate-Independent Young's Modulus

Application Note

Jennifer Hay

Introduction

The problem of determining intrinsic film properties from indentation data that are influenced by both film and substrate is an old one. If the film is thick enough to be treated as a bulk material, then the analysis of Oliver and Pharr (1992) is typically used [1]. When the film is so thin that indentation results at all practical depths are substantially affected by the substrate, the influence of the substrate must be accurately modeled in order to extract the properties of the film alone. Since 1986, many such models have been proposed [2-12].

In 1992, Gao, Chiu, and Lee proposed a simple approximate model for substrate influence. They derived two functions, I_0 and I_1, to govern the transition in elastic properties from film to substrate [5]. Beginning with his Ph.D. dissertation in 1999, Song and his colleagues took an alternate solution path which was originally suggested by Gao *et al*. but not followed [7-9]. This alternate path yielded a simpler model which is called the "Song-Pharr model" in the literature. The Song-Pharr model predicts substrate effect reasonably well when the film is more compliant than the substrate. Unfortunately, none of the available models works well when the film is stiffer than the substrate. This shortcoming motivated the present work.

Finite-element analysis (FEA) is essential to the development and verification of analytic contact models, because FEA idealizes experiment. In a finite-element model, the film thickness, film properties, and substrate properties are all well known, because they are required inputs. Also, there is little ambiguity about the true contact area under load, because it is determined from the last node(s) in contact. So before turning to experimentation, the worth of an analytic model is first assessed by means of FEA. For example, an elastic finite-element model may be constructed with a film of thickness t on a substrate, with the input properties being the Young's modulus and Poisson's ratio of the film (E_f, ν_f), and the Young's modulus and Poisson's ratio of the substrate (E_s, ν_s). Then, indentation into the material is simulated, and the simulated force-displacement data are analyzed in order to achieve a value for the Young's modulus of the film, i.e. $E_{f\text{-}out}$. What is the difference between this output value and the value that was used as an input to the finite-element model? FEA allows this question to be answered systematically over the domain of situations that might be encountered experimentally: thick films, thin films, stiff films on compliant substrates, compliant films on stiff substrates, etc. If an analytic model applied to simulated data fails to return the input properties

Agilent Technologies

with sufficient accuracy, it should not be expected to work well when applied to experimental data.

Indentation into a film-substrate system generally does not produce a contact of the same shape as would be achieved in a semi-infinite body having the same properties as the film [13]. Thus, the analysis of Oliver and Pharr [1] for predicting contact area may not yield a sufficiently accurate measure of the true contact area. When the film is more compliant than the substrate, the tendency is for the film material to "pile-up" around the face of the indenter, meaning that the Oliver-Pharr analysis will underpredict the true contact area [13]. If the film is stiffer than the substrate, the tendency is for the film to be pressed into the substrate well outside the contact area, meaning that the Oliver-Pharr analysis will overpredict the true contact area [14]. These phenomena are evident in FEA, but they do not present a problem, because the contact area is obtained from the mesh. But these phenomena can present a practical problem for the experimenter. Finite-element simulations can be used to identify experimental conditions under which such problems may arise.

In the present work, a new analytic model is presented that is informed by and improves upon previous analytic models. The new model is tested and refined by FEA over the domain $0.1 < E_f/E_s < 10$ and $4\% < h/t < 40\%$. The simulations are also used to identify the conditions under which the Oliver-Pharr analysis for determining contact error should be expected to work well. This analytic work prepares the way for future experimental verification of the model.

Theory

The present model is a development of the Song-Pharr model, which in turn, draws from the Gao model. The Song-Pharr model is illustrated schematically in Figure 1. It assumes that a column of material under the indenter, defined by the contact radius, can be isolated from the surrounding material, and treated as two springs in series, with the influence of each spring weighted according to a/t through the function I_0. Thus, the measured (or apparent) shear modulus (μ_a) is related to the shear modulus of the film (μ_f) and that of the substrate (μ_s) through this expression:

$$\frac{1}{\mu_a} = (1 - I_0)\frac{1}{\mu_s} + I_0\frac{1}{\mu_f} \qquad \text{(Eq. 1)}$$

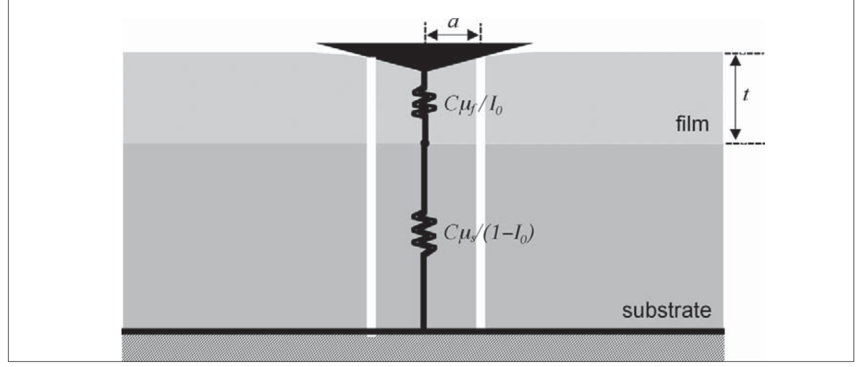

Figure 1. Schematic of the Song-Pharr model which assumes that material under the indenter can be isolated from surrounding material and treated as springs in series.

The weighting function, I_0, is that of Gao *et al* [5]. It provides a smooth transition from film to substrate. When I_0 is unity, as it is when the contact is small relative to the film thickness, then $\mu_a = \mu_f$. As the penetration increases, the value of I_0 approaches zero, which makes $\mu_a = \mu_s$. The function I_0 is plotted in Figure 2 and given by

$$I_0 = \frac{2}{\pi}\arctan\left(\frac{t}{a}\right) + \frac{1}{2\pi(1-\nu_a)}\left[(1-2\nu_a)\frac{t}{a}\ln\left(\frac{1+(t/a)^2}{(t/a)^2}\right) - \frac{t/a}{1+(t/a)^2}\right] \qquad \text{(Eq. 2)}$$

Unfortunately, the limit of $\mu_f \rightarrow \infty$ poses a problem for the Song-Pharr model [9]. As the film modulus becomes large, the apparent compliance ($1/\mu_a$) should go to zero, but Eq. 1 does not predict this. Rather, it predicts that the apparent compliance will be governed by the compliance of the substrate, meaning that the apparent compliance calculated by Eq. 1 will be too large. The root cause of the problem is that as $\mu_f \rightarrow \infty$, the material under the indenter cannot be isolated from the surrounding material, because the film offers significant lateral support. The behavior is like that of a steel drum: upon being struck, the response is governed primarily by the drum skin—its elastic properties, thickness, and boundaries—not by the near-zero compliance of the air underneath the drum skin.

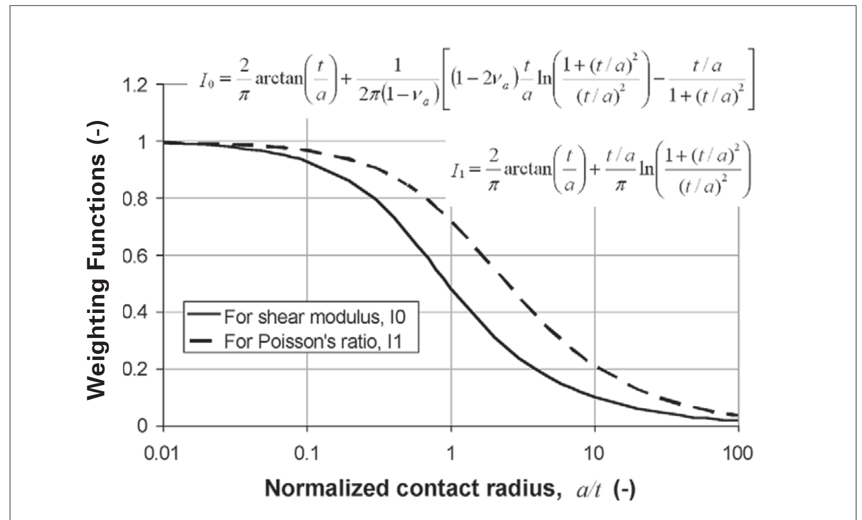

Figure 2. Gao's weighting functions I_0 and I_1 which govern the film-to-substrate transition for shear modulus and Poisson's ratio, respectively.

To improve upon the Song-Pharr model, we suppose that phenomenologically, the film can also act as a spring in parallel with the substrate as illustrated schematically in Figure 3. There are several ways to consider the sense of this configuration. First, as the film becomes stiff, it dominates the response, and this is what happens with parallel springs—the stiffer spring dominates. Second, as the film becomes thin and stiff, the deformation in the top layer of the substrate approaches that of the film. If two springs of different stiffness experience the same deformation subject to the same force, then they should be modeled as parallel. Finally, if the film provides significant lateral support, then it effectively acts on the indenter like the leaf springs which support the indenter column, and these leaf springs are well modeled by a parallel spring.

Springs in parallel are treated together by adding their stiffnesses. Thus, the proposed model is:

$$\frac{1}{\mu_a} = (1-I_0)\frac{1}{\mu_s + FI_0\,\mu_f} + I_0\frac{1}{\mu_f} \qquad \text{(Eq. 3)}$$

In the denominator of the first term on the right-hand side, the influence of the film modulus is moderated by two factors: I_0 and F. The moderation with I_0 makes the film influence degrade with depth. We also allow for moderation with the tunable constant, F, because we don't know, *a priori*, the importance of film modulus relative to that of the substrate. We shall determine the best value for the constant F using finite-element analysis.

Eq. 3 gives us the right behavior in the limits of $I_0 \longrightarrow 1$, $I_0 \longrightarrow 0$, $\mu_f << \mu_s$, and $\mu_f >> \mu_s$. When I_0 is close to 1, as it is at shallow penetration depths, the apparent modulus approaches that of the film. As I_0 approaches 0, as it does at large depths, the apparent modulus approaches the substrate modulus. In the case of a compliant film on a rigid substrate ($\mu_f << \mu_s$), Eq. 3 reduces to the Song-Pharr model (Eq. 1) for all values of I_0. Finally, when the film modulus is very large, the apparent compliance goes to zero for all values of I_0, as it should.

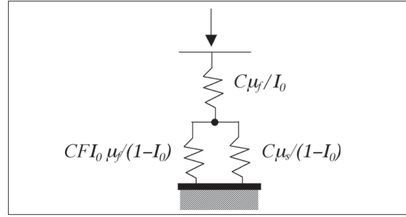

Figure 3. Schematic of the proposed model allowing the film to act in series and in parallel with the substrate.

Thus, the shear modulus of the film is calculated from the apparent value by solving Eq. 3 for μ_f:

$$\mu_f = \frac{-B + \sqrt{B^2 - 4AC}}{2A}, \text{ where} \qquad \text{(Eq. 4)}$$

$$A = FI_0$$
$$B = \mu_s - (FI_0^2 - I_0 + 1)\mu_a$$
$$C = -I_0\,\mu_a\mu_s$$

Finally, the Young's modulus of the film is calculated from the shear modulus and Poisson's ratio as

$$E_f = 2\mu_f(1+\nu_f). \qquad \text{(Eq. 5)}$$

Calculation of μ_a from standard indentation results for use in Eq. 3 requires a value for Poisson's ratio. The weighting function I_0 also utilizes Poisson's ratio. But what value should be used—that of the film or that of the substrate? To be sure, this problem is of second order, but Gao *et al.* also provided a weighting function, I_1, for handling the transition in Poisson's ratio, so that the apparent Poisson's ratio, ν_a, is calculated as

$$\nu_a = 1 - \left[\frac{(1-\nu_s)(1-\nu_f)}{1-(1-I_1)\nu_f - I_1\nu_s}\right]. \qquad \text{(Eq. 6)}$$

Eq. 6 provides the value for Poisson's ratio used in the calculation of μ_a and I_0 [7-9]. It should be noted that if film and substrate have the same Poisson's ratio (that is, if $\nu_s = \nu_f = \nu$), then Eq. 6 reduces to $\nu_a = \nu$. Gao's function I_1 is also plotted in Figure 2 and given by

$$I_1 = \frac{2}{\pi}\arctan\left(\frac{t}{a}\right) + \frac{t/a}{\pi}\ln\left(\frac{1+(t/a)^2}{(t/a)^2}\right). \qquad \text{(Eq. 7)}$$

Finite-element Analysis

Seventy axisymmetric finite-element simulations were performed using Cosmos 2.8. These simulations are summarized in Table 1. An updated Lagrangian formulation was used to handle potentially large strains. The solution was achieved in discrete time steps. At each time step, the solution was found by force control with Newton-Raphson iteration.

Some simulation inputs were fixed, and some were systematically varied in order to investigate the domain of interest. The film thickness was set to 500 nm for all simulations; indentation depth was varied in order to investigate the domain of $4\% < h/t < 40\%$. All indented materials, both film and substrate, were assigned a Poisson's ratio (ν) of 0.25 and a linear-elastic stress-strain curve. (Thus, neither the effect of plasticity nor of transition in Poisson's ratio was investigated by FEA.) The Young's modulus of the film was fixed at 10 GPa. To achieve the desired variation in E_f/E_s, the substrate modulus varied between 100 GPa ($E_f/E_s = 0.1$) and 1 GPa ($E_f/E_s = 10$). Because Poisson's ratio was set to 0.25 for all materials, the modulus ratios are the same whether expressed in terms of Young's modulus or shear modulus, i.e. $\mu_f/\mu_s = E_f/E_s$.

Simulation	Es, GPa	Maximum indenter displacement (h), nm									
1-10	100	20	40	60	80	100	120	140	160	166	174
11-20	50	20	40	60	80	100	120	140	160	166	184
21-30	20	20	40	60	80	100	120	140	160	180	200
31-40	10	20	40	60	80	100	120	140	160	180	200
41-50	5	20	40	60	80	100	120	140	160	180	200
51-60	2	20	40	60	80	100	120	140	160	180	200
61-70	1	20	40	60	80	100	120	140	160	180	200

Table I. Summary of finite-element simulations, showing values for inputs that were varied. For all simulations the indenter was a 2-dimensional version of a Berkovich diamond. For the sample, t = 500 nm, E_f = 10 GPa, and $\nu_f = \nu_s = 0.25$.

The purpose of simulations 31-40 was to verify the finite-element model. For these simulations, the finite-element model had the mesh of a film-substrate system, but with film and substrate having the same modulus (i.e. $E_f = E_s$ = 10 GPa), and so behaving as a bulk sample. Thus, the intention was to verify the general finite-element model by showing that for simulations 31-40, standard analysis of simulated data yields an output modulus that is very close to the input value.

For all simulations, the indenter was a cone having an included angle of 140.6° and an apical radius of 50 nm. This shape is the two-dimensional analogue of the common Berkovich indenter. The indenter was defined to be a linear-elastic material having the properties of diamond: E = 1140 GPa and ν_i = 0.07.

Both the indenter and the sample were meshed with four-node axisymmetric plane strain elements. For the sample, the extent of the mesh was 90 a' in both the radial and axial directions, where a', the anticipated contact radius, was calculated as the radius of the indenter at a distance from the apex that is equal to the specified indentation depth. The radial extent of the fine mesh near the contact was 1.2 a'. The radial extent of the indenter mesh was 45 a', and the axial extent was 90 a'.

The boundary conditions were specified as follows. Along the right-hand side and bottom of the sample, all nodes were rigidly fixed. Along the axis of symmetry (the left hand side of both the indenter and sample), nodes were constrained to move along the axis of symmetry only (μ_x = 0). Nodes along the top of the indenter were displaced downward by the total prescribed displacement which took place in discrete time steps. Nodes along the right-hand side of the indenter were unconstrained. The interaction between the indenter and the sample was handled as follows. The nodes along the indenter form a curve. Surface nodes on the sample were not allowed to pass to the other side of this curve (line-contact formulation). No slip was allowed between film and substrate.

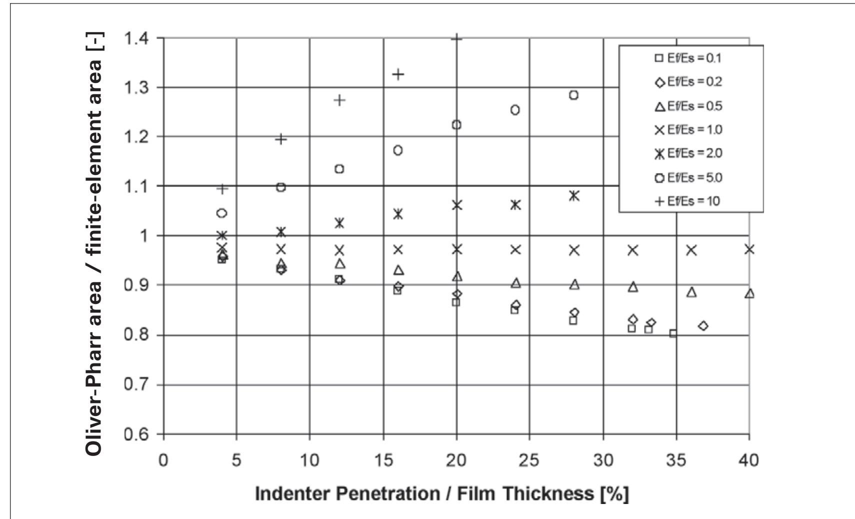

Figure 4. Evaluation of the ability to calculate contact area by the Oliver-Pharr method as a function of film/substrate mismatch and indentation depth. For Ef/Es = 1, the Oliver-Pharr method gives a contact area that is within 3% of the finite-element value.

Results

We can have confidence in the finite-element results, because application of standard analysis to the simulated data from runs 31-40 (for which E_f/E_s = 1) yields an output modulus that differs from the input value by no more than 1%. This close agreement is achieved by using contact area as calculated from the finite-element mesh, not as calculated by the Oliver-Pharr method.

One aspect of "substrate effect" is the extent to which the substrate affects the ability to determine contact area by the Oliver-Pharr method [1]. Figure 4 shows the Oliver-Pharr contact area relative to the finite-element area for all simulations. Values less than unity indicate pile-up, and values greater than unity indicate excessive sink-in. For simulations 31-40, the Oliver-Pharr method yields a contact area that is within 3% of the finite-element area; this agreement is excellent, given the simplicity of the calculation.

The error in the contact area achieved by the Oliver-Pharr method depends on whether the film or substrate is more compliant, the degree of modulus mismatch, and the indentation depth relative to the film thickness. The compliant films on stiff substrates exhibit a tendency to pile-up, meaning that the areas calculated from the Oliver-Pharr method are too small, with the severity of the problem increasing with the degree of modulus mismatch and indentation depth. The stiff films on compliant substrates exhibit a tendency to sink-in excessively, meaning that the areas calculated from the Oliver-Pharr method are too large. Again, the error magnitude increases with the degree of modulus mismatch and indentation depth. However, for the same degree of mismatch and relative indentation depth, the error for stiff films is much greater than for compliant films.

Figure 4 allows us to predict the error in modulus due to shortcomings in the Oliver-Pharr method for determining contact area. The corresponding error in modulus is half the magnitude of the error in contact area and of the opposite direction, because the calculation for modulus from indentation data depends inversely on the square root of contact area ($1/\sqrt{A}$). For example, if the calculated contact area is 10% larger than the true contact area, the resulting value of modulus will be 5% smaller than the true modulus. For compliant films ($0.1 \leq E_f/E_s < 1$), the error in modulus should be less than about 5% if the indentation depth is less than 10% of the film thickness. For moderately stiff films ($1 < E_f/E_s \leq 2$), the error in modulus should be less than 5% so long as the indentation depth is less than 20% of the film thickness. For very stiff films ($E_f/E_s > 2$) the error due

to the area calculation is substantial at all practical indentation depths. For such samples, the Oliver-Pharr method for determining contact area should not be used.

Another aspect of "substrate effect" is the composite response of the film and substrate to the indentation force. Figure 5 shows the inverse of the apparent shear modulus (hereafter: apparent compliance) as a function of normalized contact radius for film/substrate systems having the most severe modulus mismatch (E_f/E_s = 0.1 and E_f/E_s = 10). The centerline marks the true value for the film—that is, the finite-element input value. Results for stiff films on compliant substrates are plotted in grey above this centerline; results for compliant films on stiff substrates are plotted below. The open symbols are the values obtained from the finite-element simulations. Each plotted point represents a single simulation of pressing the indenter into the film to a prescribe depth and withdrawing it, then analyzing the simulated force-displacement data in the usual way, but using contact area as calculated from the finite-element mesh. The dashed curves show the apparent compliance as predicted by the Song-Pharr model (Eq. 1), given the film thickness, material properties, and contact geometry. The solid curves show the apparent compliance as predicted by the new model (Eq. 3), given the same information, and a single value for the empirical constant of F = 0.0626. (The means by which F was determined are explained subsequently.) For compliant films on stiff substrates, the Song-Pharr model and the new model are indistinguishable; they predict the finite-element results equally well. But for stiff films on compliant substrates, the new model provides a much better prediction of finite-element results. Rar, Song, and Pharr published a nearly identical plot comparing their own finite-element simulations (via ABAQUS) to the Song-Pharr model [8].

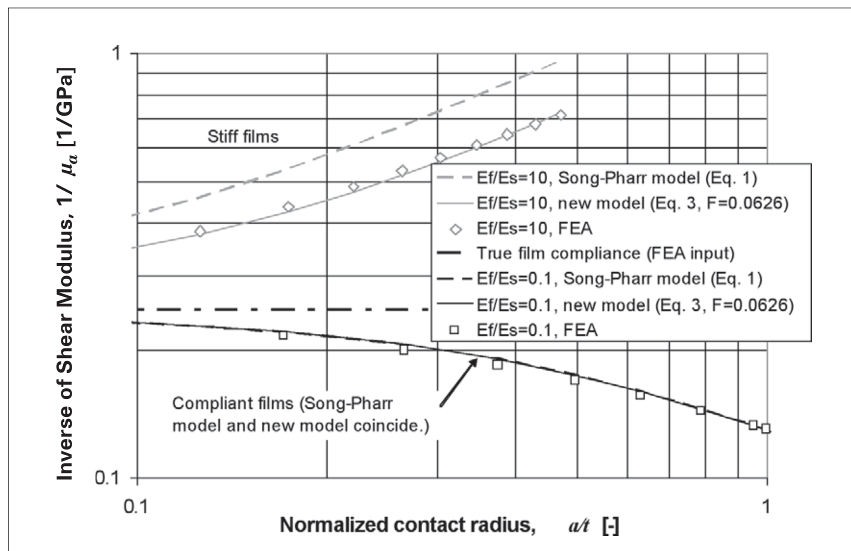

Figure 5. Comparison between two models and finite-element results for the film/substrate systems having the most severe modulus mismatch. For compliant films, the Song-Pharr model and the new model are the same; for stiff films, the new model is substantially better than the Song-Pharr model at predicting apparent compliance.

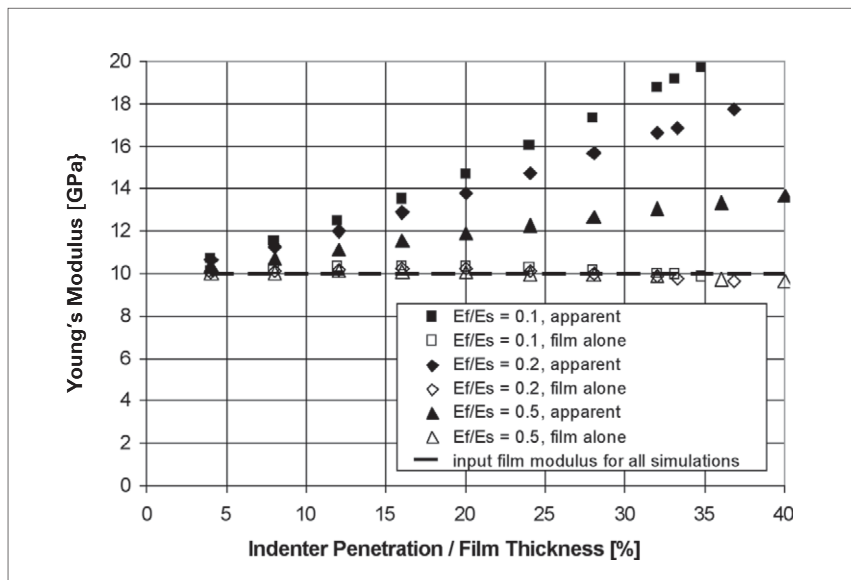

Figure 6. Young's modulus vs. normalized indentation depth for 30 simulations of indenting into compliant films (E = 10GPa) on stiff substrates. Solid symbols are substrate-affected results obtained by standard analysis; open symbols are the Young's modulus of the film, computed by Eq. 5.

The new model expressed by Eq. 3 allows us to compute the Young's modulus of the film by Eq. 5 with F = 0.0626. Figure 6 shows Young's modulus vs. normalized penetration for the 30 simulations of indentation into compliant films on stiff substrates (sims 1-30). All values have been computed using contact area as determined by the finite-element mesh. The solid symbols represent the substrate-affected modulus that would be obtained by standard analysis. The open symbols represent the film modulus as computed by Eq. 5. The values for film modulus

determined in this way agree well with the FEA input value of 10 GPa, even for penetration depths as large as 40% of the film thickness. Figure 7 shows analogous results for the 30 simulations of indentation into stiff films on compliant substrates (sims 41-70).

A single value for the empirical constant F was determined as that value which minimized the sum of the squared differences between the input Young's modulus for the film (10 GPa) and the output value as computed by Eq. 5 across all 70 finite-element simulations. Variances were not weighted. The value for the empirical constant determined in this way was $F = 0.0626$. This single value for F was used in all implementations of Eq. 3.

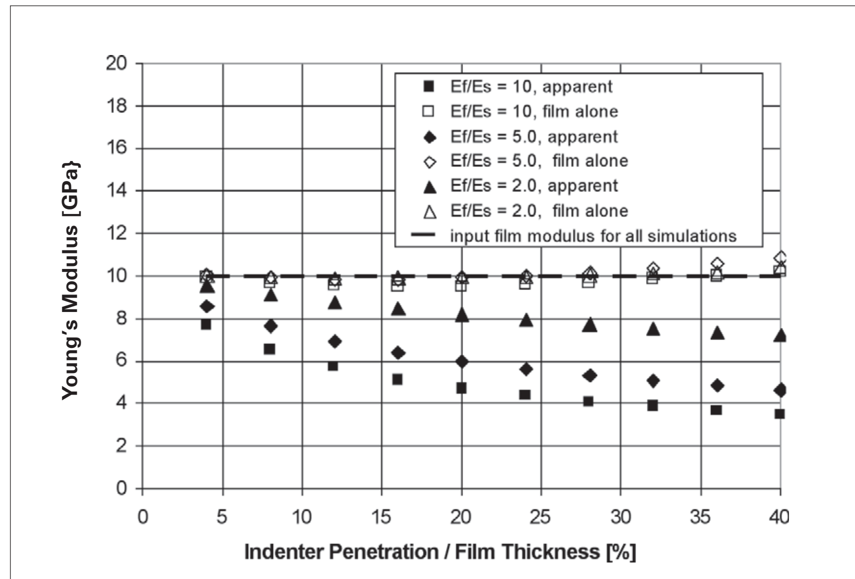

Figure 7. Young's modulus vs. normalized indentation depth for 30 simulations of indenting into stiff films (E = 10 GPa) on compliant substrates. Solid symbols are substrate-affected results obtained by standard analysis; open symbols are the Young's modulus of the film, computed by Eq. 5.

Discussion

Unfortunately, errors in Young's modulus due to errors in contact area (as determined by the Oliver-Pharr method) are easily confused with composite elastic response, because these two aspects of "substrate influence" both push the reported Young's modulus in the same direction. That is, for compliant films on stiff substrates, the tendency toward pileup can cause the Young's modulus to be artificially inflated due to the calculation of contact areas that are too small. This artificial inflation might easily be attributed to the increased composite stiffness, because both effects push the reported Young's modulus higher with increasing indentation depth. Similarly, for stiff films on compliant substrates, the tendency toward excessive sink-in can cause the Young's modulus to be artificially deflated due to the calculation of contact areas that are too large. This artificial deflation might easily be attributed to the decreased composite stiffness, because both effects push the reported Young's modulus lower with increasing indentation depth. Thus, if the Oliver-Pharr method is used to determine contact area (as it is in most commercially available instruments) then the application of Eq. 3 should be restricted to indentation depths which are less than 20% of the film thickness. But if the problem of errant contact areas were solved by means of advanced modeling or microscopy, then Eq. 3 could be used at depths as great as 40% of the film thickness.

Conclusions

An elastic film-substrate model, Eq. 3, has been proposed that accurately relates the apparent shear modulus obtained from an instrumented indentation experiment to the shear moduli of film and substrate, thus allowing the extraction of film modulus if substrate modulus and film thickness are known. The model works well for both compliant films on stiff substrates and vice versa. If the Oliver-Pharr model is used to determine the contact area, then the film-substrate model should not be used at indentation depths greater than 20% of the film thickness. However, if contact areas are determined by another method that accurately accounts for pile-up and sink-in, then the film-substrate model can be used at indentation depths as great as 40% of the film thickness.

References

1. W.C. Oliver and G.M. Pharr: An improved technique for determining hardness and elastic modulus using load and displacement sensing experiments. *J. Mater. Res.* **7,** 1564 (1992).
2. M.F. Doerner and W.D. Nix: A method for interpreting the data from depth-sensing indentation instruments. *J. Mater. Res.* **1,** 601 (1986).
3. R.B. King: Elastic analysis of some punch problems for a layered medium. *Int. J. Solid Structures* **23,** 1657 (1987).
4. T.W. Shield and D.B. Bogy: Some axisymmetric problems for layered elastic media: Part 1—Multiple region contact solutions for simply connected indenters. *J. Appl. Mech.* **56,** 798 (1989).
5. H. Gao, C.-H. Chiu, and J. Lee: Elastic contact versus indentation modeling of multi-layered materials. *Int. J. Solids Structures* **29,** 2471 (1992).
6. J. Menĉík, D. Munz, E. Quandt, E.R. Weppelmann, and M.V. Swain: Determination of elastic modulus of thin layers using nanoindentation. *J. Mater. Res.* **12,** 2475 (1997).
7. H. Song: *Selected mechanical problems in load- and depth-sensing indentation testing.* Rice University Ph. D. Thesis (1999).
8. A. Rar, H. Song, and G.M. Pharr: Assessment of new relation for the elastic compliance of a film-substrate system. *Mater. Res. Soc. Symp. Proc.* **695,** 431 (2002).
9. H. Xu and G.M. Pharr: An improved relation for the effective elastic compliance of a film/substrate system during indentation by a flat cylindrical punch. *Scripta Materialia 55,* 315 (2006).
10. S. Bec, A. Tonck, J.M. Georges, E. Georges, J.L. Loubet: Improvements in the indentation method with a surface force apparatus. *Philosophical Magazine A* **74,** 1061 (1996).
11. S. Roche, S. Bec, J.L. Loubet: Analysis of the elastic modulus of a thin polymer film. *Mater. Res. Soc. Symp. Proc.* **778,** 117 (2003).
12. J.L. Hay: Measuring substrate-independent modulus of dielectric films by instrumented indentation. *J. Mater. Res.* **23,** 667 (2009).
13. R. Saha and W.D. Nix: Effects of the substrate on the determination of thin film mechanical properties by nanoindentation. *Acta Materialia* **50,** 23 (2002).
14. W.Y. Ni and Y.T. Cheng: Modeling conical indentation in homogeneous materials and in hard films on soft substrates. *J. Mater. Res.* **20,** 521 (2005).

Nano Mechanical Systems from Agilent Technologies

Agilent Technologies, the premier measurement company, offers high-precision, modular nano-measurement solutions for research, industry, and education. Exceptional worldwide support is provided by experienced application scientists and technical service personnel. Agilent's leading-edge R&D laboratories ensure the continued, timely introduction and optimization of innovative, easy-to-use nanomechanical system technologies.

www.agilent.com/find/nanoindenter

Americas

Canada	(877) 894 4414
Latin America	305 269 7500
United States	(800) 829 4444

Asia Pacific

Australia	1 800 629 485
China	800 810 0189
Hong Kong	800 938 693
India	1 800 112 929
Japan	0120 (421) 345
Korea	080 769 0800
Malaysia	1 800 888 848
Singapore	1 800 375 8100
Taiwan	0800 047 866
Thailand	1 800 226 008

Europe & Middle East

Austria	43 (0) 1 360 277 1571
Belgium	32 (0) 2 404 93 40
Denmark	45 70 13 15 15
Finland	358 (0) 10 855 2100
France	0825 010 700* *0.125 €/minute
Germany	49 (0) 7031 464 6333
Ireland	1890 924 204
Israel	972-3-9288-504/544
Italy	39 02 92 60 8484
Netherlands	31 (0) 20 547 2111
Spain	34 (91) 631 3300
Sweden	0200-88 22 55
Switzerland	0800 80 53 53
United Kingdom	44 (0) 118 9276201

Other European Countries:
www.agilent.com/find/contactus

Product specifications and descriptions in this document subject to change without notice.

© Agilent Technologies, Inc. 2010

Printed in USA, August 31, 2010
5990-6507EN

Agilent Technologies